https://doi.org/10.5194/egusphere-2025-5270
Preprint. Discussion started: 5 December 2025

Retrieving Tropospheric Temperature and Humidity Profiles Over the Ocean Using Buoy-Based Microwave Radiometers

Zhiqian Li[1,2], Fuqing Liu[2], Shuo Jiang[2], Zhongling Zhou[2], Zhijin Qiu[1,2], Jing Zou[1,2], Tong Hu[1,2], Ke Qi[1,2], Bo Wang[1,2]✉, Bin Wang[3]✉

[1]State Key Laboratory of Physical Oceanography, Qingdao, 266061, China
[2]Institute of Oceanography instrumentation, Qilu University of Technology (Shandong Academy of Science), Jinan, 250353, China
[3]School of Information Science and Technology, Qingdao University of Science and Technology, Qingdao, 266061, China
Correspondence to: Bo Wang (bob80.wang@hotmail.com), Bin Wang (18661855732@163.com)

Abstract. The acquisition of atmospheric temperature and humidity profiles over the sea is strategically vital for meteorological forecasting, marine monitoring, and national security. Achieving their real-time, stable, and routine retrieval under complex sea conditions is a critical and urgent challenge. Traditional retrieval methods rely heavily on large historical datasets. However, marine sounding stations are sparse, making data acquisition challenging. Concurrently, buoy platforms experience wave disturbance, causing real-time variations in zenith angle observations. Without correction, this induces significant random errors in target brightness temperature. To address these issues, this paper proposes a collaborative retrieval method. This method does not rely on historical data and integrates platform attitude information. Our approach uses a multi-objective genetic algorithm to construct a small-scale joint prior database. It also incorporates an attitude error correction model, a pressure-altitude model, and a parallel optimization strategy. This fundamentally eliminates dependence on historical data. It also effectively mitigates systematic errors from buoy attitude, enhances computational efficiency, and enables real-time, routine retrieval of marine atmospheric profiles. Simulation experiments and field tests in Qingdao's Jiaozhou Bay confirm the results. Under sparse data conditions, the temperature RMSE is 2.08 K, and the humidity RMSE of 20.95%. This validates the method's stability and applicability in real marine environments. This research provides a potentially practical pathway for ocean areas with sparse radiosondes for real-time, stable, and routine detection of marine atmospheric parameters.

1 Introduction

The lower troposphere is the region where most human activities and weather phenomena take place. The systematic measurement of meteorological parameters in this region is a critical foundation for high-precision weather forecasting and climate change research. It is also essential for ensuring the efficiency of aviation, voyage, and radio communication systems (Maciejewska, 2025; Morbidelli et al., 2011). However, unprecedented challenges are presented for the precise detection of

https://doi.org/10.5194/egusphere-2025-5270
Preprint. Discussion started: 5 December 2025

atmospheric parameters due to the unique geographical characteristics and dynamic processes of the marine environment. Recent studies have further highlighted the complexity of marine atmospheric structures, particularly under extreme weather conditions such as tropical cyclones. For instance, Wei et al. (2025) demonstrated that vertical wind shear can induce significant asymmetry in atmospheric duct distributions, underscoring the spatial and temporal variability of atmospheric properties in oceanic regions.

The primary bottlenecks are the sparse distribution of oceanic sounding stations and the inherent limitations of traditional atmospheric retrieval methods, contributing to a significant observational gap in the atmospheric boundary layer (Cimini et al., 2020). Data acquisition is made extremely difficult by the sparse distribution. The limitations are particularly evident when dealing with marine dynamic environments. Specifically, these limitations include an excessive reliance on large amounts of historical data and an inability to effectively account for potential interference and correction issues. These issues are caused by changes in the attitude of the detection platform on observational signals.

Currently, various mainstream methods are used for atmospheric parameter profiling retrieval. These include the Bayesian maximum probability estimation algorithm (Clough et al., 2005), one-dimensional variational retrieval methods (Hewison, 2007), physically based retrieval methods based on radiative transfer theory (Zhou et al., 2024; Liu et al., 2024; Gaffard and Hewison, 2003; Reinhardt et al., 2009), and statistical retrieval methods (Zheng, 2010). Neural-network algorithms have also gained increasing attention (Renju et al., 2023). While high computational accuracy can theoretically be achieved with physical retrieval methods, their inherently large computational requirements severely limit real-time performance. Statistical retrieval methods are effective in terrestrial environments where sufficient data is available. However, their strong reliance on historical data makes them struggle in marine regions with limited data. Neural-network algorithms demonstrate outstanding performance due to their powerful nonlinear mapping capabilities. However, traditional neural network models, such as the classic BP neural network, generally require a large amount of training data (Hu et al., 2023; Jiménez and Eriksson, 2016). This high data requirement conflicts sharply with the limited ability to obtain field data in the unique environment of the ocean. As a result, their training effects and retrieval performance are significantly limited (Yao and Guan, 2022; Mahdianpari et al., 2021). Previous studies have confirmed this point. For example, Turner et al. (2007) noted that physical retrieval methods, while accurate, are inefficient. Decker et al. (1978) made significant progress in ground-based detection. However, the adaptability of their method in marine environments remains a key concern. Guiraud et al. (1979) revealed the detection capabilities of absorption spectra at different frequencies. In their Arctic region study, Candlish et al. (2012) explicitly pointed out that the accuracy of ship-based platform data is significantly reduced when using traditional neural-network-based retrieval of atmospheric profiles. This is due to changes in attitude and insufficient on-site data. Recent studies also suggest that even state-of-the-art reanalysis data like ERA5 may exhibit systematic biases under complex marine weather conditions such as tropical cyclones (Wei et al., 2025), further emphasizing the need for observation-driven profiling methods in data-sparse oceanic environments. These studies collectively highlight a core issue: how to effectively overcome errors caused by platform attitude and achieve high-precision, high-efficiency retrieval of atmospheric parameter profiles. This is especially important in marine environments characterized by sparse data and complex platform motion.

https://doi.org/10.5194/egusphere-2025-5270
Preprint. Discussion started: 5 December 2025

In this context, ground-based microwave radiometers (MWR) have emerged as a cutting-edge remote sensing technology. They are capable of capturing atmospheric microwave radiation information in real-time and continuously. This enables the retrieval of key parameters, such as atmospheric temperature and humidity profiles, and atmospheric refractive index. On the other hand, buoys are flexible, real-time monitoring platforms. They can integrate multi-parameter measurement functions and offer the unique advantages of long-term, uninterrupted, and all-weather operation. This can effectively compensate for the observational deficiencies caused by the sparse distribution of traditional oceanic sounding stations (Roemmich et al., 2009; Cronin et al., 2023; Liu et al., 2019; Fang, 2018). Consequently, an effective approach to addressing the scarcity of tropospheric data in marine environments is the combination of advanced ground-based microwave radiometer technology with flexible buoy monitoring platforms. Industry initiatives have previously explored this potential, such as the deployment of the first floating microwave radiometer (Haun, 2017). In the academic field, several studies have also explored the application of microwave radiometers in marine environments. For instance, Schnitt et al. (2024) and Griesche et al. (2020) demonstrated ship-based profiling capabilities, while Yan et al. (2022) focused on improving retrieval algorithms for ocean-based platforms. More recently, Cimini et al. (2025) reviewed the capability of microwave radiometers for offshore wind energy applications, highlighting that while onshore retrievals show high correlation (>0.9) with radiosondes (Cimini et al., 2003), offshore retrievals are significantly challenged by platform motion and data sparsity, necessitating advanced calibration and elevation scanning strategies.

Therefore, this study deploys a ground-based microwave radiometer on an ocean buoy platform. Through incorporating platform attitude correction methods and applying multi-objective optimization algorithms, a history-independent retrieval model is constructed to address the challenges above. Through simulation experiments and field sea trials, the method's performance, retrieval accuracy, and universality are comprehensively evaluated. Its potential for application in real marine environments is also assessed.

2 Instrument, Platform, and Sites

2.1 The QFW-6000 microwave radiometric profiler

The QFW-6000 microwave radiometer, developed by the China Electronics Technology Corporation No.22 Research Institute, is employed in this study. The microwave radiometer is installed on the buoy's upper platform. It is used to detect, receive, and analyze microwave brightness temperatures from the zenith direction. Brightness temperature is observed from the zenith direction using 16 microwave channels. Of these, eight channels in the K-band (22.24–31.4 GHz) are primarily used to detect water vapor. Eight channels in the V-band (51.26–58.0 GHz) are used to detect atmospheric oxygen. The device has a vertical resolution of 25 m in the 0–0.5 km range, 50 m in the 0.5–2 km range, and 250 m in the 2–10 km range. Its maximum detection distance is 10 km. The QFW-6000 Microwave Radiometer features integrated temperature, humidity, and pressure sensors that provide real-time surface thermodynamic data for in-situ calibration and retrieval correction. Additionally, it incorporates

https://doi.org/10.5194/egusphere-2025-5270
Preprint. Discussion started: 5 December 2025

a rain intensity sensor and an infrared cloud sensor to facilitate weather identification during rainy and cloudy conditions. The physical appearance of the QFW-6000 microwave radiometer is shown in Fig. 1.

Figure 1: The QFW-6000 microwave radiometric profiler developed by the CETC No.22 Research Institute was deployed for the experiment. The instrument features a K-band and V-band receiver for profiling tropospheric temperature and humidity.

2.2 The Buoy Platform

The buoy platform was developed by the Institute of Oceanographic Instrumentation, Shandong Academy of Sciences. The buoy has a UFO or disc-shaped appearance. It is constructed from a highly durable and corrosion-resistant, fully sealed, welded steel structure. The buoy body is 10 m in diameter and weighs approximately 30 tons. After modification, the platform can stably accommodate key equipment, such as the QFW-6000 microwave radiometer and attitude sensors. This adaptation to the marine environment ensures reliable data collection. The buoy's middle section houses a battery and an instrument compartment. Its exterior is composed of six buoyancy chambers to ensure stability and safety.

2.3 Attitude Sensor

The attitude of the buoy is a key parameter affecting the measurement accuracy of microwave radiometers during maritime navigation. Attitude sensors are used to measure the roll angles and pitch angles of the measurement platform. The zenith angle θ can be obtained by substituting the attitude sensor output data into the derived calculation formula for the buoy attitude and zenith angles. The calculation formula for the buoy's zenith angle is as follows eq. (1):

$$\cos\theta = \cos\alpha\cos\beta\ , \tag{1}$$

By substituting this observed zenith angle into the atmospheric microwave radiation equation, the oblique path brightness temperature can be obtained. This enables attitude compensation and correction, which in turn improves retrieval accuracy.

https://doi.org/10.5194/egusphere-2025-5270
Preprint. Discussion started: 5 December 2025

2.4 The Sites

The Jiaozhou Bay area off the coast of Qingdao (36.0721540° N, 120.3047530° E) was used as the sea trial research area. As shown in Fig.2, the retrieval data of microwave radiometer atmospheric temperature and humidity profiles were systematically analyzed. For comparative analysis and validation, radiosonde data from the Qingdao Observatory (Station ID: 54857; 36.0702040° N, 120.3331640° E) in the upper-air sounding database of the University of Wyoming, USA, were selected (http://weather.uwyo.edu/upperair/bufrraob.shtml). The two sites are 2.5 km apart. Therefore, the microwave radiometer data and the radio sounding data can be considered co-located observation data. The sea trial experimental environment is shown in Fig.3.

Figure 2: Map of the Jiaozhou Gulf region showing the experimental sites. The red triangle indicates the location of the Buoy-based Microwave Radiometer (36.0721540° N, 120.3047530° E), and the yellow circle represents the Radiosonde Station (36.0702040° N, 120.3331640° E). The two instruments are separated by a distance of approximately 2.5 km. Basemap from Cartopy Quadtree Tiles.

https://doi.org/10.5194/egusphere-2025-5270
Preprint. Discussion started: 5 December 2025

Figure 3: Schematic of the sea trial experimental setup on the 10-meter diameter buoy platform. Key components include: the attitude sensor (top left) for monitoring platform roll and pitch; the QFW-6000 atmospheric brightness temperature measurement unit (bottom left) installed on the upper deck; and the OceanBuoy Host (right) for data aggregation and transmission. The red circles in the central photograph indicate the mounting positions of the sensors on the buoy structure.

In the Jiaozhou Bay area, the modified and liquid nitrogen-calibrated QFW-6000 microwave radiometer and attitude sensor will be attached to a 10-meter buoy platform according to the layout shown in Fig.3. Brightness temperature and tilt angle will be collected simultaneously at the buoy's top level. Data will be aggregated via the serial port to the OceanBuoy Host. After data retrieval is completed, results will be transmitted back to the shore station.

3 Data, Model, and Method

3.1 The Data Source

Observed brightness temperature data were derived from the QFW-6000 microwave radiometer. The sounding data are from the University of Wyoming sounding station database. Specifically, data from the Qingdao Meteorological Observatory (Station ID:54857) are used. The data are collected twice daily at 00:00 and 12:00 UTC. Attitude data are obtained from the attitude sensor in the buoy platform. The sensor collects attitude data every second. The zenith angle data are derived using the buoy attitude angle and the zenith angle calculation formula. Using the microwave radiation transfer equation, brightness temperature data along the inclined path can be corrected to that of the zenith path.

3.2 Atmospheric Microwave Radiation Transmission Model

Calculating the absorption coefficient is a critical step in achieving precise retrieval. This is done during the atmospheric microwave radiation transmission process. Currently, commonly used models include: the MPM89 and MPM93 models by

https://doi.org/10.5194/egusphere-2025-5270
Preprint. Discussion started: 5 December 2025

Liebe et al. (1993), the Rosenkranz98 and Rosenkranz02 models by Rosenkranz (2016), and the MonoRTM model by the U.S. Atmospheric Environment Research Center (Clough et al., 2005). In this study, the ITU-R P.676-13 model was selected to calculate the atmospheric absorption coefficients in the microwave band (ITU). This model was developed by the International Telecommunication Union-Radiocommunication Sector (ITU-R). This model provides detailed fits for the absorption characteristics of various gases (e.g., water vapor and oxygen) at different frequencies.

After the atmospheric absorption coefficient is obtained, it is used as an input parameter in the atmospheric microwave radiation transfer equation (see Sect.3.3). This is done to calculate brightness temperature values at different altitude layers and observation angles. Specifically, the atmospheric absorption coefficients in the K and V bands are calculated using the ITU-R P.676-13 model. Simulated brightness temperature is calculated using ITU-R P.676-13. They are then passed as key input parameters to the atmospheric microwave radiation transfer equation. The resulting brightness temperature values are compared with measured brightness temperatures. This is done to drive the retrieval process.

3.3 Atmospheric Microwave Radiation Transmission Equation

This study is based on the theoretical foundations of atmospheric parameter retrieval. It also follows Kirchhoff's law of thermal radiation. The focus is on the energy exchange characteristics between the atmosphere and environmental electromagnetic radiation. In the field of microwave remote sensing, this principle reflects the positive correlation between an object's absorption and radiation capabilities at specific frequencies (Konabe et al., 2021). It is also closely linked to the microscopic physical mechanisms by which gas molecules release or absorb electromagnetic waves during quantum energy level transitions. In the microwave frequency band (300 MHz–3000 GHz), electromagnetic waves exhibit both wave-like and particle-like properties. Their excellent ability to penetrate the atmosphere makes them an indispensable tool for atmospheric remote sensing. Research indicates (Wentz and Meissner, 2016) that atmospheric absorption is primarily caused by the combined effects of oxygen molecules (O_2), water vapor molecules (H_2O), and liquid water. This occurs within the frequency range of 1-100 GHz. Among these, strong absorption spectral lines are formed by oxygen molecules near approximately 60 GHz. Their absorption intensity exhibits a high correlation with atmospheric temperature distribution. Water vapor molecules exhibit a significant absorption peak at 22.235 GHz, which is highly sensitive to changes in humidity. Liquid water causes attenuation of microwave radiation transmission through continuous background absorption effects (Payne et al., 2011; Liebe et al., 1992; Cadeddu et al., 2007).

Within the K/V band range, the absorption effects of water droplets in clouds on microwave radiation are particularly significant. The intensities far exceed those of scattering effects. Therefore, the scattering component can be neglected in radiation transmission models. When a microwave radiometer performs upward (zenith) observations, the brightness temperature reaching it can be approximated as a sum. This approximation is based on the Rayleigh-Jeans approximation and the atmospheric radiation characteristics. The sum is composed of the cosmic background radiation's contribution after atmospheric attenuation and the atmospheric radiation emitted outward. The theoretical expression is written as (Renju et al., 1993)eq.(2):

https://doi.org/10.5194/egusphere-2025-5270
Preprint. Discussion started: 5 December 2025

$$T = T_\infty \exp(-\int_0^\infty k_a \sec\theta dz) + \int_0^\infty T(z) k_a \exp\left(-\int_0^z k_a \sec\theta dz\right) \sec\theta dz, \quad (2)$$

Among these variables is the brightness temperature observed by the microwave radiometer. θ is the zenith angle. T_∞ is the cosmic background brightness temperature, which is generally taken as 2.73 K. $T(z)$ is the atmospheric temperature at altitude z. $\sec\theta$ assuming each layer of the atmosphere is uniform, the oblique path satisfies the secant relationship, where is the atmospheric absorption coefficient. This coefficient is the sum of the absorption coefficients of each component in the atmosphere.

3.4 The Retrieval Algorithm Construction

3.4.1 Data Preprocessing

This study conducted a comprehensive statistical analysis of the routine radiosonde data. We aimed to accurately obtain the normal distribution patterns of temperature and humidity. Based on the theory of normal distribution confidence intervals, abnormal-sounding data deviating from the normal range were excluded. Additionally, radiosonde data are influenced by factors such as ascent speed and wind. This leads to inconsistent measurement data at different altitudes. To address these data-mismatch issues, linear interpolation was performed on the collected radiosonde data.

Furthermore, pressure profiles were obtained using actual ground-based pressure sensor data combined with empirical pressure-altitude formulas. The specific pressure-altitude formula is eq.(3):

$$P = 0.5 \times 101.3 \times \left\{ (5.3788 \times 10^{-9} \quad -1.1975^{-4} \quad 1) \begin{pmatrix} H^2 \\ H \\ 1 \end{pmatrix} + \left[1 - 0.0255 \times \frac{H}{1000} \left(\frac{6357}{6357 + \frac{H}{1000}} \right) \right] \right\}^{5.256}, \quad (3)$$

Here, H indicates local sea level height in meters, and P denotes the local average atmospheric pressure in kPa.

3.4.2 Construction of Atmospheric Prior Experience Database

The preprocessed radiosonde data were interpolated to the same 83 height levels as the microwave radiometer using linear interpolation. A monthly statistical analysis revealed that temperature and humidity (T, H) at each height layer conformed to a normal distribution. The variables were substituted into the formulas $N\left(\mu_i^T, \sigma_i^T\right)$ and $N\left(\mu_i^{\mathrm{H}}, \sigma_i^{\mathrm{H}}\right)$. It was found that atmospheric temperature followed a perfect normal distribution, while relative humidity exhibited a skewed distribution. The skewed variables were then transformed by taking their natural logarithms. They were then fitted to a normal distribution. Within the interval $\left[\mu_i^T - 2\sigma_i^T, \mu_i^T + 2\sigma_i^T\right]$, the sounding data values were set to $\begin{cases} T_i^{\min} = \mu_i^T - 2\sigma_i^T, T_i^{\max} = \mu_i^T + 2\sigma_i^T \\ H_i^{\min} = \mu_i^H - 2\sigma_i^H, H_i^{\max} = \max(H_i) \end{cases}$. This eliminated anomalous-sounding data and completed the construction of the empirical database.

https://doi.org/10.5194/egusphere-2025-5270
Preprint. Discussion started: 5 December 2025

3.4.3 NOGA-II

Addressing the challenges of sparse data, significant dynamic platform disturbances, and the high computational cost of traditional inversion methods requiring large samples in ocean observations, this study builds upon the NOGA-II framework. It implements essential enhancements in three key areas: small-sample constraints, embedded physical laws, and dynamic attitude compensation. Supplemented by parallel computing and systematic error correction, the approach adapts to real-world scenarios characterized by sparse ocean observation data and unstable platforms. For the first time, it achieves high-precision temperature and humidity profile inversion under small-sample conditions and dynamic ocean environments. Specifically: (1) A small-sample prior knowledge base is constructed, significantly reducing reliance on massive training data through statistical modeling and physical boundary constraints; (2) Physical laws such as atmospheric lapse rates are introduced as hard constraints, effectively suppressing inversion results that violate physical principles; (3) Integrated attitude sensor data to compensate in real-time for zenith angle deviations caused by platform sway, enhancing robustness in dynamic conditions. Furthermore, employing a parallel computing architecture and systematic error correction mechanism, the single-run inversion time was reduced to the second level under parameter configurations of 175 individuals, 10 generations, a crossover probability of 0.9, and a mutation probability of 0.2, meeting the requirements for real-time maritime applications. The specific inversion workflow is designed as follows:

1. Construction of the Objective Function

The core of the retrieval process is an established multi-objective optimization problem. The objective is to minimize the difference between simulated and measured brightness temperatures. Physical constraints are introduced to ensure the reasonableness of the retrieval results. Specifically, the objective function $\begin{cases} min\,|\tilde{T}_{ret}^{22\mathrm{GHz}} - T_{obs}^{22\mathrm{GHz}}| \\ min\,|\tilde{T}_{ret}^{58\mathrm{GHz}} - T_{obs}^{58\mathrm{GHz}}| \end{cases}$ is constructed based on the difference between simulated and measured brightness temperatures from microwave radiometers in the K/V bands. Here, $\tilde{T}_{ret}^{22\mathrm{GHz}}$ denotes the simulated brightness temperature in the microwave radiometer's K-band, $T_{obs}^{22\mathrm{GHz}}$ represents the measured brightness temperature in the K-band channel, $\tilde{T}_{ret}^{58\mathrm{GHz}}$ indicates the simulated brightness temperature in the V-band, $T_{obs}^{58\mathrm{GHz}}$ denotes the measured brightness temperature of the microwave radiometer's V-band channel. Additionally, atmospheric physical characteristics, such as temperature and humidity lapse rates $\begin{cases} \underset{i\in N, i\leqslant 83}{min}|T_{i+1} - T_i| \leqslant \delta_1 \\ \underset{i\in N, i\leqslant 83}{min}|H_{i+1} - H_i| \leqslant \delta_2 \end{cases}$, are incorporated into the constraint system. Here, N denotes the maximum value obtained for i, δ_1 represents the maximum temperature lapse rate, and δ_2 denotes the maximum humidity lapse rate. Given the general trend that temperature and humidity typically decrease with increasing altitude in the troposphere, these lapse rate trends are used as constraints. This limits non-physical results that may arise during the retrieval process. By integrating these objectives and constraints. This transforms the retrieval problem into an optimization problem, which requires the solution of an optimal profile.

2. Initialization of the Population

https://doi.org/10.5194/egusphere-2025-5270
Preprint. Discussion started: 5 December 2025

First, reasonable value ranges are defined for the temperature and humidity variables at each altitude layer using the constructed atmospheric prior experience database. Within this probability boundary, an initial population is generated through random sampling. Each individual represents a complete set of potential temperature-humidity profile solutions. Next, the fitness of each individual in the population is assessed. To ensure population diversity and convergence, key techniques from the non-dominance sorting genetic algorithm (NSGA-II) are employed. These techniques, such as density sorting and Pareto dominance, are used to evaluate and select the offspring population.

3. Parallel Computing Optimization

We introduced parallel computing technology to optimize algorithm efficiency. Specifically, we used a master-slave parallel mode. This mode divides the population into multiple sub-populations, which are then assigned to different CPUs for independent calculations. The master processor manages task allocation and result aggregation. The slave processors complete their calculations and report the results back. This approach significantly improves the retrieval efficiency.

4. Obtaining the Optimal Solution

After the genetic algorithm completes its preset number of iterations, a set of multiple Pareto optimal solutions is produced. To select the final optimal solution from this set, a hybrid reconstruction strategy is employed. First, the extreme optimal values for each objective function are identified. These are the solutions in the Pareto optimal solution set that minimize the difference between the simulated and measured brightness temperatures in the K/V band. Subsequently, these solutions with extreme optimal values are mixed and reconstructed across different objectives. This generates a solution with the best overall performance. This solution serves as the final retrieval result.

5. System Error Correction

To further improve the accuracy of the retrieval results, a system error correction method is designed and introduced. A dataset of 38 independent samples is randomly sampled. This is then divided into a training set (80 %) and a test set (20 %). The training set is used to establish the system error model. Meanwhile, the test set serves as an independent dataset to validate the effectiveness of the correction method. For temperature and humidity, the systematic error $E(h)$ at each height layer h is calculated as follows eq.(4) and eq.(5):

$$E_T(h) = \frac{1}{M}\sum_{i=1}^{M}\left(T_{ret,i}(h) - T_{obs,i}(h)\right), \tag{4}$$

$$E_H(h) = \frac{1}{M}\sum_{i=1}^{M}\left(H_{ret,i}(h) - H_{obs,i}(h)\right), \tag{5}$$

Among these variables: $E_T(h)$ and $E_H(h)$ are the systematic errors in temperature and humidity at height h. M is the number of samples in the training set. $T_{ret,i}(h)$ and $H_{ret,i}(h)$ are the original retrieval values at height h for the i-th sample, while $T_{obs,i}(h)$ and $H_{obs,i}(h)$ are the corresponding sounding observation values. After the systematic error model is established using this method, it is applied to correct all retrieval profiles. The corrected temperature and humidity profiles, $T_{corr}(h)$ and $H_{corr}(h)$, are obtained by subtracting the corresponding systematic errors from the original retrieval profiles, $T_{ret}(h)$ and $H_{ret}(h)$. For temperature and humidity, the $T_{corr}(h)$ and $H_{corr}(h)$ calculated as follows eq.(6) and eq.(7):

https://doi.org/10.5194/egusphere-2025-5270
Preprint. Discussion started: 5 December 2025

$$T_{corr}(h) = T_{ret}(h) - E_T(h)\ , \tag{6}$$

$$H_{corr}(h) = H_{ret}(h) - E_H(h)\ , \tag{7}$$

The temperature and humidity profiles corrected for the system errors are the final retrieval results.

4 Results

To comprehensively evaluate the performance and suitability of the proposed models for marine environments, microwave radiometer observation experiments were conducted on a buoy platform. This was done in the coastal waters of Jiaozhou Bay, Qingdao (36.0721540° N, 120.3047530° E). The models include the tropospheric temperature and humidity profile retrieval model and the buoy platform zenith compensation correction model. During the experiment, 38 sets of valid observational data were obtained. These data were compared with radio sounding data from the Qingdao Meteorological Observatory (Station ID: 54857) for validation. The sounding data are from the Wyoming State University sounding database (36.0702040° N, 120.3331640° E). The two observation points are 2.5 km apart. Therefore, their data can be considered co-located observations. This provides reliable reference true values for model validation.

To quantitatively assess the performance of the proposed retrieval model, the RMSE was calculated. The RMSE is the difference between the model retrieval results and the radiosonde data. RMSE serves as a standard metric for measuring the difference between model predictions and actual observations. The calculation formula is as follows eq.(8):

$$RMSE = \sqrt{\frac{1}{m}\sum_{i=1}^{m}(y' - y)^2}, \tag{8}$$

In this equation, m represents the number of samples used in the calculation. y'represents the temperature and humidity profiles obtained through the model's retrieval. y represents the radio sounding observation data used as the true value for verification.

https://doi.org/10.5194/egusphere-2025-5270
Preprint. Discussion started: 5 December 2025

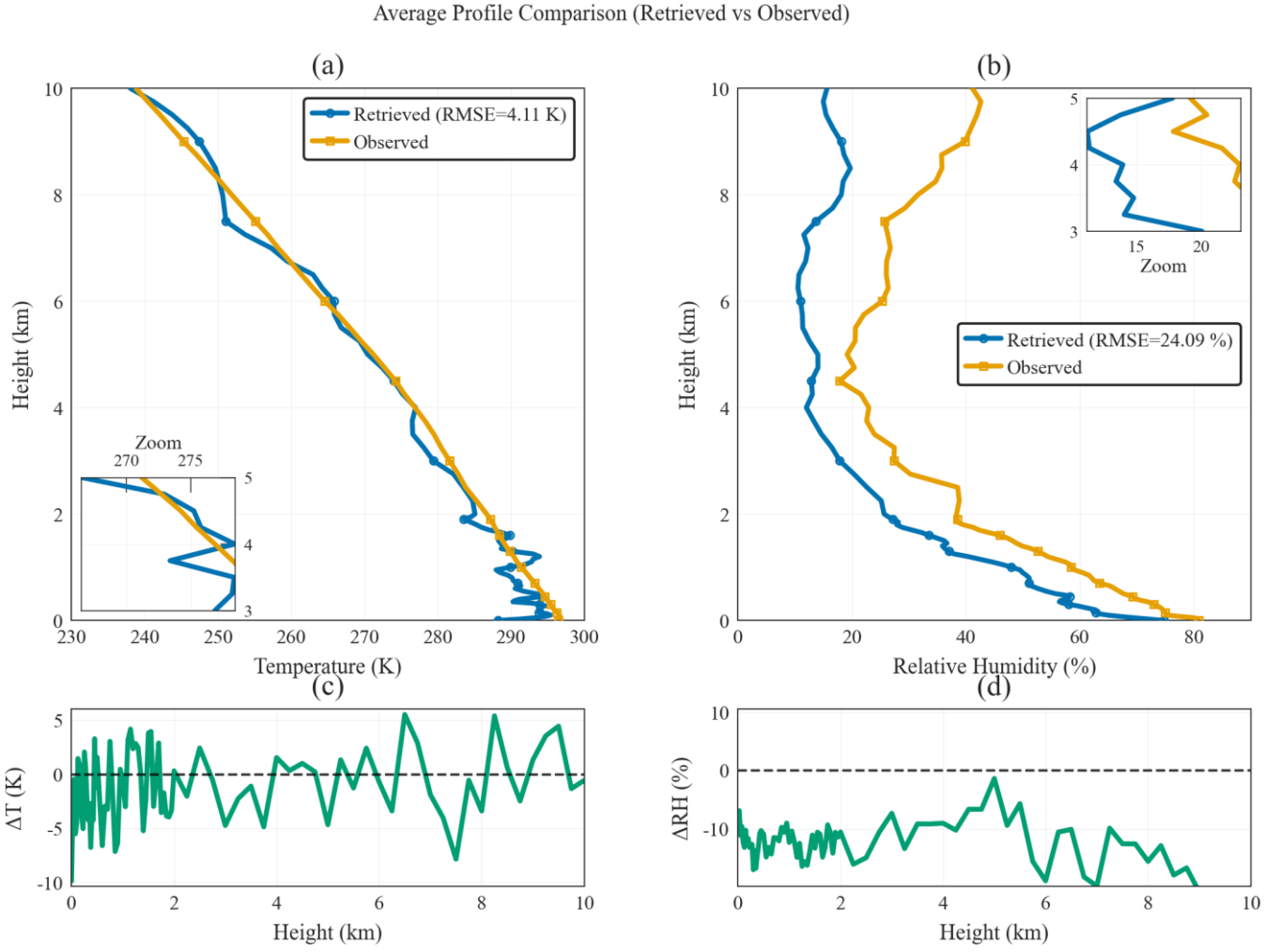

Figure 4: Statistical comparison of atmospheric profiles between the uncorrected NOGA-II retrievals and radiosonde observations. Panels (a) and (b) display the mean temperature and relative humidity profiles, respectively. The blue solid lines represent the initial retrievals from the buoy-based Microwave Radiometer (MWR) using the NOGA-II algorithm before systematic error correction, while the orange-yellow solid lines denote the co-located reference observations from the Qingdao Radiosonde Station (ID: 54857). Panels (c) and (d) illustrate the vertical distribution of the mean retrieval bias (Retrieved minus Observed) for temperature and humidity. The statistics are derived from the average of 38 valid matchups collected during the field campaign in Jiaozhou Bay from August 22 to September 23, 2023.

Figure 4 shows the average comparison between the temperature and humidity profiles (blue solid lines) retrieved by the NOGA-II algorithm without any systematic error correction and the true values from the Jiaozhou Bay radiosonde observations (orange-yellow solid lines), along with the distribution of their difference with height. Fig. 4(a) and 4(c) reveal that the temperature profile exhibits a trend highly consistent with the sounding data within the near-surface layer at 0–2 km, particularly in Fig. 4(c), where deviations approach the zero line, indicating good retrieval accuracy in the near-surface layer. However, with increasing altitude, the retrieval profile exhibits a systematic positive deviation of 1.5–3 K between 3 and 6 km, peaking at 4–5 km. This aligns precisely with the height at which sensitivity decreases in the trough region of the microwave

https://doi.org/10.5194/egusphere-2025-5270
Preprint. Discussion started: 5 December 2025

weighting function. Beyond 6 km, the deviation recedes to 1–2 K but persists as a weaker positive bias, indicating that while the upper-level accuracy improves, the systematic error remains unresolved. The deviation patterns in the relative humidity profiles (Fig.4(b) and 4(d)) are more complex: a positive deviation of 5–15% exists between 1–2 km, transitioning to a systematic negative deviation of 10–25% between 2–5 km, peaking near 4 km. This layer coincides with the sensitivity decline zone of the 22 GHz channel, where samples with cloud liquid water path greater than 0.2 mm exhibit the most significant residual influence. Above 5 km, the negative bias gradually converges but persists as a weaker 5–10% deviation, indicating vertical propagation of the mid-level dry bias. Overall, the uncorrected profile's systematic errors exhibit height-selective distribution in Fig.4(c) and (d). Temperature errors concentrate between 3–6 km, while humidity errors cluster between 2–5 km. Though their peak regions overlap, their shapes differ significantly. This further highlights the mesosphere as a "vulnerable zone" for simultaneous temperature-humidity retrieval, necessitating targeted correction through height-dependent error modeling.

Overall, the uncorrected profiles capture the general distribution characteristics of tropospheric temperature and humidity. However, significant local systematic errors require further correction through error modeling. Therefore, this study incorporates systematic error correction processing.

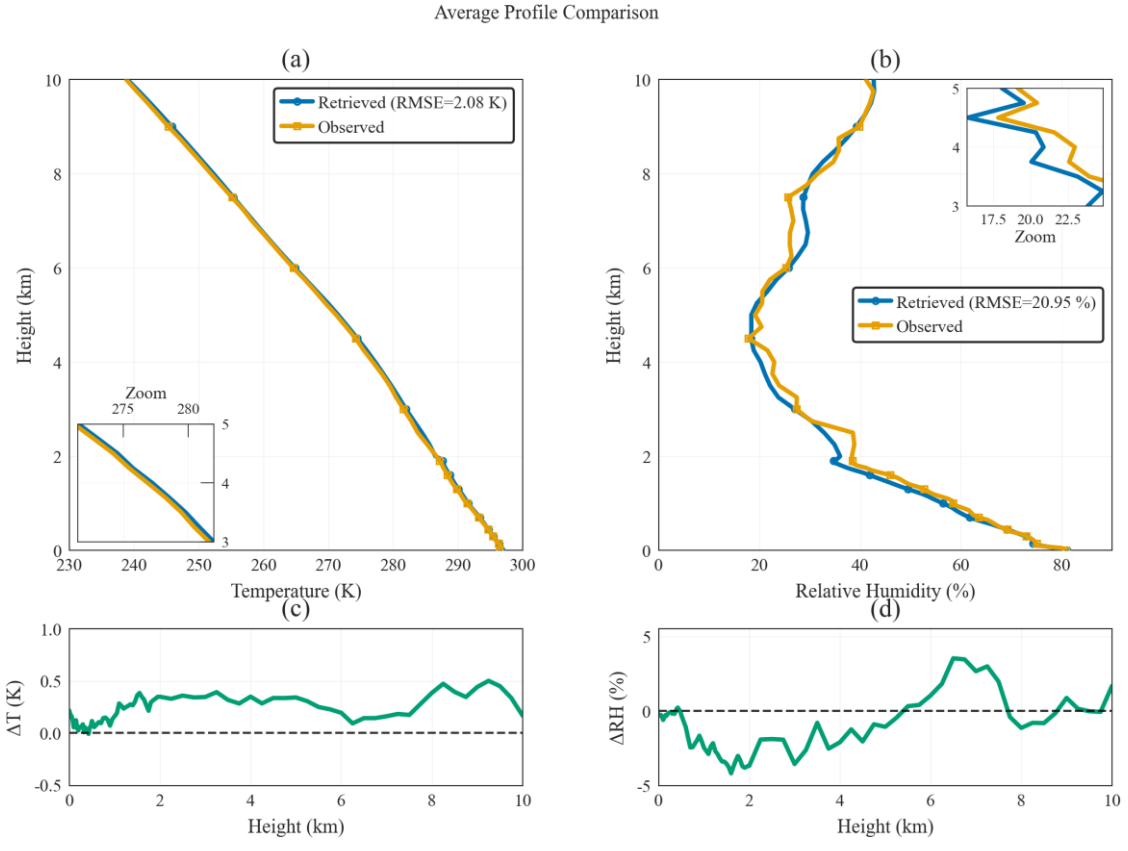

Figure 5: Comparison of retrieval results after applying the systematic error correction model. Panels (a) and (b) display the corrected temperature and relative humidity profiles, respectively. The blue solid lines represent the MWR retrieval results

https://doi.org/10.5194/egusphere-2025-5270
Preprint. Discussion started: 5 December 2025

corrected by subtracting the systematic error profiles $E_T(h)$ and $E_H(h)$ as defined in Eqs. (4) and (5). The orange-yellow solid lines represent the reference radiosonde observations. Panels (c) and (d) display the residual error profiles after correction. Based on the 38 valid matchups, the Root Mean Square Error (RMSE) for the corrected profiles is reduced to 2.08 K for temperature and 20.95% for humidity across the 0–10 km vertical range.

Figure 5 presents the comparison between the NOGA-II retrieved profiles (after systematic error correction) and the radiosonde observations. Compared to the pre-correction results, the retrieval accuracy has significantly improved. To further quantify the correction effectiveness and the overall retrieval performance, a detailed statistical summary of the 38 validation cases is provided in Table 1.

Table 1. Statistical summary of retrieval performance for temperature and humidity profiles across different altitude layers based on 38 validation cases.

Variable	Altitude Layer	MBE	RMSE	Correlation (*R*)
Temperature (K)	0-2 km	0.17	2.14	0.83
	2-10 km	0.30	2.34	0.99
	Overall (0-10 km)	**0.22**	**2.08**	**0.99**
Relative Humidity (%)	0-2 km	-1.71	18.79	0.57
	2-10 km	-0.17	25.25	0.27
	Overall (0-10 km)	**-1.12**	**20.95**	**0.66**

Temperature Retrieval Performance: As shown in Fig. 5(a) and Table 1, the corrected temperature retrieval demonstrates excellent accuracy, with an overall correlation coefficient (*R*) of 0.99 and an RMSE of 2.08 K across the full vertical profile. The residual error profile in Fig. 5(c) confirms that the systematic bias has been largely eliminated (Overall MBE = 0.22 K). It is worth noting that while the correlation coefficient for the 0–2 km layer (*R*=0.83) is slightly lower than that of the 2–10 km layer (*R*=0.99), the RMSE indicates superior absolute accuracy in the near-surface layer (2.14 K vs. 2.34 K). The exceptionally high correlation in the 2–10 km range is largely driven by the significant temperature lapse rate across the troposphere, which dominates the statistical calculation. In contrast, the 0–2 km layer exhibits more complex thermal structures, which are inherently smoothed by the radiometric retrieval, leading to a slightly lower correlation despite the higher measurement precision.

Humidity Retrieval Performance: For relative humidity (Fig. 5(b)), the overall RMSE is 20.95% with a correlation of 0.66. As illustrated in Fig. 5(d) and quantified in Table 1, the systematic bias has been effectively minimized (Overall MBE = -1.12%). However, the correlation coefficients for humidity are lower compared to temperature (0.57 for 0–2 km and 0.27 for 2–10 km). This is attributed to three primary factors: (1) Vertical Resolution: Radiosondes capture high-frequency variations and sharp humidity gradients (e.g., cloud layers), whereas microwave radiometer retrievals are inherently smooth; (2) Spatial Mismatch: The high spatial variability of water vapor, combined with the 2.5 km separation between the buoy and the radiosonde station, introduces unavoidable discrepancies; and (3) Sensitivity Decay: In the upper troposphere (2–10 km), the water vapor content is low, and the sensitivity of the K-band channels decreases, making the retrieval more susceptible to noise. Despite these

https://doi.org/10.5194/egusphere-2025-5270
Preprint. Discussion started: 5 December 2025

physical limitations, the RMSE values indicate that the proposed method provides valuable humidity information for marine monitoring.

In summary, the sea trial results validate the effectiveness and feasibility of the proposed method. By constructing a small-scale prior experience database and integrating platform attitude information, the NOGA-II algorithm successfully overcomes reliance on extensive historical data. The statistical performance confirms that this approach provides a robust solution for real-time, stable retrieval of tropospheric atmospheric parameters in data-sparse marine environments.

5 Discussion

This study addresses the issues of sparse marine data and the reliance of traditional retrieval methods on large amounts of historical data. A method to retrieve tropospheric temperature and humidity profiles using a ground-based microwave radiometer is proposed and preliminarily validated. The method is based on a multi-objective genetic algorithm (NOGA-II). It has been successfully deployed on a buoy platform, thereby expanding the marine application scenarios of ground-based microwave radiometers. The core contribution of this study is the construction of a small-scale joint prior experience database for temperature and relative humidity. This effectively overcomes the excessive reliance of traditional methods on large amounts of historical training data. Additionally, the robustness and accuracy of retrieval results in dynamic marine environments have been enhanced. This was done by integrating a pressure-altitude model and a buoy attitude compensation mechanism.

Simulation experiments and field tests in the Jiaozhou Bay area have thoroughly validated the effectiveness and feasibility of this method. Notably, the comprehensive statistical analysis of the 38 validation cases demonstrates an overall RMSE of 2.08 K for temperature and 20.95% for relative humidity. The profiles were retrieved by the NOGA-II algorithm. This confirms the potential for high-precision retrieval of atmospheric profiles in marine regions with sparse sounding stations. The average profile comparison shown in Fig.4 indicates that the retrieved profiles generally align well with sounding observation data. This is particularly true near the surface and in the upper troposphere. However, some fluctuations and deviations exist in the middle troposphere (2-8 km). These are closely related to the detection mechanism of the microwave radiometer. Due to the low sensitivity of the atmospheric microwave weighting function in its valley region, the retrieval accuracy in the middle troposphere is easily challenged. This systematic deviation is consistent with the findings of Cimini et al. (2006), who attributed similar biases in this altitude range to uncertainties in the oxygen absorption model. Especially for water vapor, its rapid vertical changes and complex layered structure exceed the constraints of the limited prior experience database. This leads to significant fluctuations in the retrieval results in this region. However, overall, this method demonstrates significant potential for application.

However, due to the high cost and short window period of maritime synchronous sounding experiments, only 38 sets of valid matching profiles were obtained. The limited sample size restricts the extrapolation of results to larger marine areas and extreme weather conditions. Future work will focus on two areas: data fusion and the expansion of observation networks. First,

https://doi.org/10.5194/egusphere-2025-5270
Preprint. Discussion started: 5 December 2025

by increasing the number of buoys deployed, a maritime observation network will be established. This will achieve broader and more precise monitoring of marine atmospheric parameters. Second, multi-source data fusion techniques will be actively explored. This involves combining buoy observation data with satellite microwave / GNSS remote sensing data. This not only alleviates data scarcity but also provides richer assimilation data for numerical weather forecasting, further enhancing marine meteorological forecasting capabilities. Additionally, transfer learning methods will be adopted to improve the model's generalizability further.

In terms of algorithm optimization, the atmospheric prior experience database and multi-objective optimization strategy (NOGA-II) provide preliminary and effective constraints. However, there is still room for further improvement. The constraints include boundary and interlayer constraints for the retrieval algorithm. Future research can explore the introduction of more comprehensive physical constraints. This will further reduce retrieval uncertainty and improve accuracy. Additionally, the settings of evolutionary parameters in the NOGA-II algorithm have a critical impact on convergence speed and global optimization capability. These parameters include the genetic operator and mutation operator. Subsequent work can employ more systematic simulation optimization strategies to fine-tune these parameters. The aim is to achieve higher retrieval accuracy and computational efficiency.

6 Conclusion

This study addresses challenges posed by data sparsity and platform attitude in traditional marine atmospheric detection. An innovative method is proposed to retrieve tropospheric atmospheric parameter profiles. The core work and main conclusions are summarized as follows:

(1) A retrieval model independent of historical data was established: A small-scale joint prior experience database for temperature and relative humidity was innovatively constructed. This was based on limited historical sounding data and a pressure-height model. It provides reasonable boundary constraints for subsequent retrieval algorithms. This mechanism effectively overcomes the reliance of traditional methods on massive historical data. It offers a solution for marine environments where data acquisition is challenging.

(2) Development and validation of a retrieval model based on a multi-objective genetic algorithm: A convective tropospheric temperature and humidity profile co-retrieval method was proposed. This method is based on a multi-objective genetic algorithm (NOGA-II). It integrates the microwave radiometer observed brightness temperature with physical constraints into a multi-objective optimization problem. It also significantly improves retrieval efficiency through parallel computation optimization. Field sea trial results demonstrate that this method can achieve high-precision temperature and humidity profile retrieval. The RMSE values are 2.08 K for temperature and 20.95 % for relative humidity. This provides an effective solution for data-scarce marine environments.

(3) Integrated application of microwave radiometers on buoy platforms was achieved: Ground-based microwave radiometers were successfully integrated with buoy platforms. Changes in zenith angle caused by buoy sway were compensated for using

https://doi.org/10.5194/egusphere-2025-5270
Preprint. Discussion started: 5 December 2025

attitude sensors. This effectively improved the accuracy of marine observations. This integrated innovative method provides a new technical approach for meteorological detection in mesoscale marine regions. This is particularly useful in marine areas with sparse traditional sounding stations. It enables real-time, continuous atmospheric monitoring.

Overall, the method proposed in this study provides new insights into addressing the challenges of tropospheric atmospheric parameter detection in marine environments. Future research will continue to focus on three areas: the refinement and optimization of algorithms, multi-source data fusion, and the expansion of observation networks. The aim is to further enhance the model's universality and application value.

Author contribution

Zhiqian Li was responsible for conceptualization, methodology, software (model code development), data curation, and validation. He also wrote the original draft with support from all co-authors. Fuqing Liu contributed to the investigation (experimental execution) and data curation, and participated in the review and editing of the manuscript. She also performed a critical review and editing of the manuscript. Shuo Jiang, Zhongling Zhou, Zhijin Qiu, Jing Zou, Tong Hu, and Ke Qi contributed to the investigation (field experiments) and provided essential resources and technical support. Bo Wang was responsible for project management, fundraising, reviewing and editing. Bin Wang was also responsible for project management, reviewing and editing.

Competing interests

The authors declare that they have no conflict of interest.

Acknowledgements

The authors thank the University of Wyoming for providing the radiosonde data.

Code and data availability

The source code, sea-trial observational dataset, and processing scripts related to this paper have been uploaded to Zenodo under a CC-BY-4.0 license (https://doi.org/10.5281/zenodo.17389912). The runtime environment is Python 3.9. Historical radiosonde data were obtained from the University of Wyoming public database (Qingdao station, ID 54857) and are freely available at http://weather.uwyo.edu/upperair/bufrraob.shtml.

https://doi.org/10.5194/egusphere-2025-5270
Preprint. Discussion started: 5 December 2025

Financial support

This study was financially supported by the National Key R&D Program of China (Grant no. 2022YFC3104202), the National Natural Science Foundation of China (Grant nos. 42206188 and 42176185), the Shandong Provincial Key R&D Program (Competitive Platform) (Grant nos. 2023CXPT015), the National Cooperation Special Project for Science, Education, and Industry Integration Pilot Program: Research on Digital Twin System for Atmospheric Waveguides in the Yellow and Bohai Sea (Grant nos. 2024GH05), the Major Innovation Projects of the Science-Education-Industry Integration Pilot Program: the Development and Application Demonstration of a Shipborne Lidar-Based Marine Atmospheric Duct Detection System (Grant nos. 2025ZDZX05) and Research Development and Demonstration of Key Technologies and Equipment for Intelligent Calibration and Validation of Ocean Satellite Remote Sensing (Grant nos. 2025ZDYS01), the Major Scientific Research Project for the Construction of State Key Laboratory at Qilu University of Technology (Shandong Academy of Sciences) (Grant nos. 2025ZDGZ01).

References

Maciejewska, A.: Use of Tropospheric Delay in GNSS-Based Climate Monitoring—A Review, Remote Sensing, 17, 1501-1529, https://doi.org/10.3390/rs17091501, 2025.

Morbidelli, R., Corradini, C., Saltalippi, C., and Flammini, A.: Atmospheric Stability and Meteorological Scenarios as Inputs to Air Pollution Transport Modeling, Water Air & Soil Pollution, 218, 275-281, https://doi.org/10.1007/s11270-010-0640-5, 2011.

Wei, C., Zhao, X., Zhu, X., Yang, P., Liu, Y., Chen, Y., and Wang, D.: Vertical wind shear induced asymmetry on atmospheric duct distribution in the context of tropical cyclones, Science China Earth Sciences, https://doi.org/10.1007/s11430-025-1660-1, 2025.

Cimini, D., Haeffelin, M., Kotthaus, S., Löhnert, U., Martinet, P., O'Connor, E., Walden, C., Collaud Coen, M., and Preissler, J.: Towards the profiling of the atmospheric boundary layer at European scale—introducing the COST Action PROBE, *Bulletin of Atmospheric Science and Technology*, 1, 23–42, https://doi.org/10.1007/s42865-020-00003-8, 2020.

Roemmich, D., Johnson, G. C., Riser, S., Davis, R., Gilson, J., Owens, W. B., Garzoli, S. L., Schmid, C., and Ignaszewski, M.: The Argo Program: Observing the Global Ocean with Profiling Floats, Oceanography, 22, 34-43, https://doi.org/10.5670/oceanog.2009.36, 2009.

Clough, S. A., Shephard, M. W., Mlawer, E. J., Delamere, J. S., Iacono, M. J., Cady-Pereira, K., Boukabara, S., and Brown, P. D.: Atmospheric radiative transfer modeling: a summary of the AER codes, Journal of Quantitative Spectroscopy and Radiative Transfer, 91, 233-244, https://doi.org/10.1016/j.jqsrt.2004.05.058, 2005.

https://doi.org/10.5194/egusphere-2025-5270
Preprint. Discussion started: 5 December 2025

Hewison, T. J.: 1D-VAR Retrieval of Temperature and Humidity Profiles From a Ground-Based Microwave Radiometer, IEEE Transactions on Geoscience & Remote Sensing, 45, 2163-2168, https://doi.org/10.1109/TGRS.2007.898091, 2007.

Zhou, S., Wei, Y., Lu, P., Yu, G., Wang, S., Jiao, J., Yu, P., and Zhao, J.: A Deep Learning Gravity Inversion Method Based on a Self-Constrained Network and Its Application, Remote Sensing, 16, 995-1010, https://doi.org/10.3390/rs16060995, 2024.

Liu, W., Wang, H., Xi, Z., and Wang, L.: Physics-Informed Deep Learning Inversion with Application to Noisy Magnetotelluric Measurements, Remote Sensing, 16, 62-82, https://doi.org/10.3390/rs16010062, 2024.

Gaffard, C. and Hewison, T.: Radiometrics MP3000 Microwave Radiometer Trial Report, http://tim.hewison.org/TR26.pdf, 2003.

Reinhardt, C., Kuga, Y., Jaruwatanadilok, S., and Ishimaru, A.: Improving bit-error-rate performance of the free-space optical communications system with channel estimation based on radiative transfer theory, IEEE Journal on Selected Areas in Communications, 27, 1591-1598, https://doi.org/10.1109/JSAC.2009.091209, 2009.

Zheng, S.: Ocean duct inversion from radar clutter using variation adjoint and regularization method (II): inversion experiment, Acta Physica Sinica,59,3912, https://doi.org/10.7498/aps.59.3912, 2010.

Renju, R., Raju, C. S., Swathi, R., and Milan, V. G.: Retrieval of atmospheric temperature and humidity profiles over a tropical coastal station from ground-based Microwave Radiometer using deep learning technique, Journal of Atmospheric and Solar-Terrestrial Physics, 249,106094, https://doi.org/10.1016/j.jastp.2023.106094, 2023.

Hu, J., Wu, J., Petropoulos, G. P., Bao, Y., Liu, J., Lu, Q., Wang, F., Zhang, H., and Liu, H.: Temperature and Relative Humidity Profile Retrieval from Fengyun-3D/VASS in the Arctic Region Using Neural Networks, Remote Sensing, 15, 1648, https://doi.org/10.3390/rs15061648, 2023.

Jiménez, C. and Eriksson, P.: A neural network technique for inversion of atmospheric observations from microwave limb sounders, Radio Science, 36, 941-953, https://doi.org/10.1029/2000RS002561, 2016.

Yao, S. and Guan, L.: Comparison of Three Convolution Neural Network Schemes to Retrieve Temperature and Humidity Profiles from the FY4A GIIRS Observations, Remote Sensing, 14, 5112, https://doi.org/10.3390/rs14205112, 2022.

Mahdianpari, M., Ghanbari, H., Mohammadimanesh, F., and Homayouni, S.: A Meta-Analysis of Convolutional Neural Networks for Remote Sensing Applications, IEEE Journal of Selected Topics in Applied Earth Observations and Remote Sensing, 14, 3602-3613, https://doi.org/10.1109/JSTARS.2021.3065569, 2021.

Turner, D. D., Clough, S. A., Liljegren, J. C., Clothiaux, E. E., and Gaustad, K. L.: Retrieving Liquid Wat0er Path and Precipitable Water Vapor From the Atmospheric Radiation Measurement (ARM) Microwave Radiometers, IEEE Transactions on Geoence and Remote Sensing, 45, 3680-3690, https://doi.org/10.1109/TGRS.2007.903703, 2007.

Decker, M. T., Westwater, E. R., and Guiraud, F. O.: Experimental Evaluation of Ground-Based Microwave Radiometric Sensing of Atmospheric Temperature and Water Vapor Profiles, Journal of Applied Meteorology, 17, 1788-1795, https://doi.org/10.1175/1520-0450(1978)017%3C1788:EEOGBM%3E2.0.CO;2, 1978.

https://doi.org/10.5194/egusphere-2025-5270
Preprint. Discussion started: 5 December 2025

Guiraud, F. O., Howard, J., and Hogg, D. C.: A Dual-Channel Microwave Radiometer for Measurement of Precipitable Water Vapor and Liquid, IEEE Transactions on Geoscience Electronics, 17, 129-136, https://doi.org/10.1109/TGE.1979.294639, 1979.

Candlish, L. M., Raddatz, R. L., Asplin, M. G., and Barber, D. G.: Atmospheric Temperature and Absolute Humidity Profiles over the Beaufort Sea and Amundsen Gulf from a Microwave Radiometer, Journal of Atmospheric & Oceanic Technology, 29, 1182-1201, https://doi.org/10.1175/JTECH-D-10-05050.1, 2012.

Wei, C., Zhao, X., Liu, Y., Yang, P., Zhou, Z., and Chen, Y.: Bias Analysis and Correction of ERA5 Reanalysis in the Context of Tropical Cyclones, Journal of Geophysical Research: Atmospheres, 130, https://doi.org/10.1029/2024JD042737, 2025.

Cronin, M. F., Anderson, N. D., Zhang, D., Berk, P., Wills, S. M., Serra, Y., Kohlman, C., Sutton, A. J., Honda, M. C., and Kawai, Y.: PMEL Ocean Climate Stations as Reference Time Series and Research Aggregate Devices, Oceanography, 36, 8, https://doi.org/10.5670/oceanog.2023.224, 2023.

Liu, L., Liao, Z., Chen, C., Chen, J., and Liu, T.: A Seabed Real-Time Sensing System for In-Situ Long-Term Multi-Parameter Observation Applications, Sensors, 19, 1255, https://doi.org/10.3390/s19051255, 2019.

Fang, H., Callafon, R. A., and Cortés, J.: Estimation-Based Ocean Flow Field Reconstruction Using Profiling Floats, Offshore Mechatronics Systems Engineering, https://doi.org/10.1201/9781315185378-8, 2018.

Haun, E.: World's First Floating Microwave Radiometer, Marine Technology News, available at: https://www.marinetechnologynews.com/news/world-first-floating-microwave-544561 (last access: 22 November 2025), 2017.

Schnitt, S., Foth, A., Kalesse-Los, H., Mech, M., Acquistapace, C., Jansen, F., Löhnert, U., Pospichal, B., Röttenbacher, J., Crewell, S., and Stevens, B.: Ground- and ship-based microwave radiometer measurements during EUREC4A, Earth Syst. Sci. Data, 16, 681–700, https://doi.org/10.5194/essd-16-681-2024, 2024.

Griesche, H. J., Seifert, P., Ansmann, A., Baars, H., Barrientos Velasco, C., Bühl, J., Engelmann, R., Radenz, M., Zhenping, Y., and Macke, A.: Application of the shipborne remote sensing supersite OCEANET for profiling of Arctic aerosols and clouds during Polarstern cruise PS106, Atmos. Meas. Tech., 13, 5335–5358, https://doi.org/10.5194/amt-13-5335-2020, 2020.

Yan, H., Zhao, Y., and Chen, S.: An Improved 1D-VAR Retrieval Algorithm of Temperature Profiles from an Ocean-Based Microwave Radiometer, J. Mar. Sci. Eng., 10, 641, https://doi.org/10.3390/jmse10050641, 2022.

Cimini, D., Gandoin, R., Fiedler, S., Acquistapace, C., Balotti, A., Gentile, S., Geraldi, E., Knist, C., Martinet, P., Nilo, S. T., Pace, G., Pospichal, B., and Romano, F.: Atmospheric stability from numerical weather prediction models and microwave radiometer observations for onshore and offshore wind energy applications, Atmos. Meas. Tech., 18, 2041–2067, https://doi.org/10.5194/amt-18-2041-2025, 2025.

Cimini, D., Shaw, J. A., Han, Y., Westwater, E. R., Irisov, V., Leuski, V., and Churnside, J. H.: Air temperature profile and air-sea temperature difference measurements by infrared and microwave scanning radiometers, Radio Sci., 38, 8045, https://doi.org/10.1029/2002RS002632, 2003.

https://doi.org/10.5194/egusphere-2025-5270
Preprint. Discussion started: 5 December 2025

Konabe, S., Nishihara, T., and Miyauchi, Y.: Theory of exciton thermal radiation in semiconducting single-walled carbon nanotubes, Opt. Lett., 46, 3021-3024, https://doi.org/10.1364/OL.430011, 2021.

Wentz, F.J.; Meissner, T.: Atmospheric absorption model for dry air and water vapor at microwave frequencies below 100GHz derived from spaceborne radiometer observations, Radio Science, 51, 381-391, https://doi.org/10.1002/2015RS005858, 2016.

Payne, V. H., Mlawer, E. J., Cady-Pereira, K. E., and Moncet, J. L.: Water Vapor Continuum Absorption in the Microwave, IEEE Transactions on Geoscience & Remote Sensing, 49, 2194-2208, https://doi.org/10.1109/TGRS.2010.2091416, 2011.

Liebe, H. J., Rosenkranz, P. W., and Hufford, G. A.: Atmospheric 60-GHz oxygen spectrum: New laboratory measurements and line parameters, Journal of Quantitative Spectroscopy and Radiative Transfer, 48, 629-643, https://doi.org/10.1016/0022-4073(92)90127-P, 1992.

Cadeddu, M. P., Payne, V. H., Clough, S. A., Cady-Pereira, K., and Liljegren, J. C.: Effect of the Oxygen Line-Parameter Modeling on Temperature and Humidity Retrievals From Ground-Based Microwave Radiometers, IEEE Transactions on Geoscience & Remote Sensing, 45, 2216-2223, https://doi.org/10.1109/TGRS.2007.894063, 2007.

Renju, R., Raju, C. S., Swathi, R., and V.G, M.: Retrieval of atmospheric temperature and humidity profiles over a tropical coastal station from ground-based Microwave Radiometer using deep learning technique, Journal of Atmospheric and Solar-Terrestrial Physics, 249, 106094, https://doi.org/10.1016/j.jastp.2023.106094, 2023.

Liebe, H. J., Hufford, G. A., and Cotton, M. G.: Propagation modeling of moist air and suspended water/ice particles at frequencies below 1000 GHz, AGARD 52nd Specialists' Meeting of the Electromagnetic Wave Propagation Panel, Palma de Mallorca, Spain, 17–21, 1993.

Rosenkranz, P. W.: Water vapor microwave continuum absorption: A comparison of measurements and models, Radio Science, 34, 1025-1025, https://doi.org/10.1029/98RS01182, 2016.

Clough, S. A., Shephard, M. W., Mlawer, E. J., Delamere, J. S., Iacono, M. J., Cady-Pereira, K., Boukabara, S., and Brown, P. D.: Atmospheric radiative transfer modeling: a summary of the AER codes, Journal of Quantitative Spectroscopy and Radiative Transfer, 91, 233-244, https://doi.org/10.1016/j.jqsrt.2004.05.058, 2005.

International Telecommunication Union (ITU). P.676 : Attenuation by atmospheric gases and related effects. 2022. ITU. Available at: https: //www. itu. int/rec/R-REC-P. 676-13-202208-I/en.

Cimini, D., Hewison, T. J., Martin, L., Güldner, J., Gaffard, C., and Marzano, F. S.: Temperature and humidity profile retrievals from ground-based microwave radiometers during TUC, *Meteorologische Zeitschrift*, 15, 45–56, https://doi.org/10.1127/0941-2948/2006/0099, 2006.